IMMUNOBIOLOGY

A mouse model recapitulating human monoclonal heavy chain deposition disease evidences the relevance of proteasome inhibitor therapy

Amélie Bonaud,[1,2] Sébastien Bender,[1,2] Guy Touchard,[3] Corinne Lacombe,[2,4] Nivine Srour,[1] Laurent Delpy,[1] Christelle Oblet,[1] Anne Druilhe,[1] Nathalie Quellard,[2,5] Vincent Javaugue,[2,3] Michel Cogné,[1] Frank Bridoux,[1,2,3] and Christophe Sirac[1,2]

[1]Centre National de la Recherche Scientifique, UMR 7276, Université de Limoges, Limoges, France; [2]Centre National de Référence Amylose AL et Autres Maladies par Dépôt d'Immunoglobulines Monoclonales, Centre Hospitalier Universitaire de Limoges, Limoges, France; and [3]Service de Néphrologie et Transplantation, [4]Service d'Immunologie, and [5]Service d'Anatomo-Pathologie, Centre Hospitalier Universitaire de Poitiers, Poitiers, France

Key Points

- We created the first transgenic mouse model recapitulating the early pathologic features of Randall-type heavy chain deposition disease.
- Production of a truncated immunoglobulin heavy chain heightens plasma cell sensitivity to bortezomib via a terminal unfolded protein response.

Randall-type heavy chain deposition disease (HCDD) is a rare disorder characterized by glomerular and peritubular amorphous deposits of a truncated monoclonal immunoglobulin heavy chain (HC) bearing a deletion of the first constant domain (CH1). We created a transgenic mouse model of HCDD using targeted insertion in the immunoglobulin κ locus of a human HC extracted from a HCDD patient. Our strategy allows the efficient expression of the human HC in mouse B and plasma cells, and conditional deletion of the CH1 domain reproduces the major event underlying HCDD. We show that the deletion of the CH1 domain dramatically reduced serum HC levels. Strikingly, even with very low serum level of truncated monoclonal HC, histologic studies revealed typical Randall-type renal lesions that were absent in mice expressing the complete human HC. Bortezomib-based treatment resulted in a strong decrease of renal deposits. We further demonstrated that this efficient response to proteasome inhibitors mostly relies on the presence of the isolated truncated HC that sensitizes plasma cells to bortezomib through an elevated unfolded protein response (UPR). This new transgenic model of HCDD efficiently recapitulates the pathophysiologic features of the disease and demonstrates that the renal damage in HCDD relies on the production of an isolated truncated HC, which, in the absence of a LC partner, displays a high propensity to aggregate even at very low concentration. It also brings new insights into the efficacy of proteasome inhibitor-based therapy in this pathology. (*Blood*. 2015;126(6):757-765)

Introduction

Tissue deposition of a monoclonal immunoglobulin fragment frequently complicates plasma cell disorders.[1,2] Among the wide spectrum of renal diseases associated with monoclonal gammopathies, Randall-type monoclonal immunoglobulin deposition disease (MIDD) is a multisystemic disorder with prominent renal manifestations including glomerular proteinuria and renal failure.[1,3-5] Kidney lesions in MIDD are characterized by nonamyloid amorphous linear deposits of a monoclonal immunoglobulin fragment along tubular, and in most cases, vascular and glomerular basement membranes (BMs). Nodular glomerulosclerosis and diffuse thickening of tubular BMs are commonly observed.[3,6] The most frequent type of MIDD is related to deposition of monoclonal light chain (LC) (LCDD), mostly of the κ isotype, but deposits composed of monoclonal heavy chain (HC) only (HCDD) or of light and heavy chain (LHCDD) have been also described.[3,7] Most reported cases of HCDD were characterized by γHC deposits.[4,5,8-11]

The mechanisms involved in the deposition of monoclonal Ig fragments in MIDD remain poorly understood. Structural peculiarities of the V domains of nephrotoxic LCs in LCDD have been suggested to govern their propensity to form insoluble aggregates that precipitate in extracellular spaces, including the presence of hydrophobic residues in the solvent-exposed complementary determining region, *N*-glycosylation, or small protein truncation.[7,12-16] Few studies also revealed a striking elevated isoelectric point of LCDD LCs compared with other pathogenic LCs, which may facilitate interactions with anionic proteoglycans of renal basement membranes.[17,18] In HCDD, the most striking molecular characteristic of the pathogenic HC is the deletion of the first constant (CH1) domain, invariably found by immunofluorescence studies of kidney biopsies and molecular studies of bone marrow.[8,9,11,19] In the absence of LC association, deletion of the CH1 domain appears to be a prerequisite for the secretion of an isolated HC, precluding its retention in the endoplasmic reticulum (ER) by the interaction with the GRP78/Bip chaperone.[20-22] The V domain also plays a critical role in the pathogenesis of HCDD. Indeed, to date, HC tissue deposition has never been reported in HC disease, a condition

Submitted February 28, 2015; accepted June 23, 2015. Prepublished online as *Blood* First Edition paper, June 25, 2015; DOI 10.1182/blood-2015-03-630277.

The online version of this article contains a data supplement.

The publication costs of this article were defrayed in part by page charge payment. Therefore, and solely to indicate this fact, this article is hereby marked "advertisement" in accordance with 18 USC section 1734.

associated with various lymphoproliferative disorders and characterized by a partial or complete deletion of the VH domain.[23]

Seminal studies by Herrera and colleagues have highlighted a specific phenotypic modification of mesangial cells on exposure to LCDD LCs.[24-29] These changes appeared similar to those observed in diabetic nephropathy, which features glomerular lesions close to those observed in MIDD.[30,31] LCDD LCs were shown to induce the production of transforming growth factor β and platelet-derived growth factor β, leading to an increased production of extracellular matrix (ECM) proteins including the unconventional tenascin-C together with an inhibition of the matrix metalloproteinase 7 production/activity.[25-28,30,32,33] This profound ECM remodeling is supposed to contribute, together with the monoclonal immunoglobulin deposits, to the pattern of nodular glomerulosclerosis frequently observed in MIDD. However, it remains difficult to depict the pathophysiologic mechanisms involved in MIDD in the absence of reliable in vivo experimental models. We previously developed models in which secreting cells producing pathogenic human LCs (isolated from patients with either LCDD or renal Fanconi syndrome) were grafted to mice. These models featured renal lesions similar to those observed in the respective patients, validating the reproducibility of the human diseases in mice and the specific involvement of the V domains in the propensity for tissue deposition.[34,35] However, the poor general condition and short survival of animals due to rapid tumor growth prevented full characterization and therapeutic investigations. To overcome these problems, we recently created a transgenic mouse model overexpressing a human LC from a patient with LC-associated Fanconi syndrome.[36] We targeted insertion of the human LC gene in the mouse κ locus, allowing a continuous high production of the LC plasma cells. This model accurately reproduced the pathologic features of the disease and permitted physiologic explorations due to the otherwise good general condition of the animals.

In the present study, we used a similar strategy to generate a transgenic model of Randall-type MIDD by targeted insertion in the κ locus of a *γ1HC* gene isolated from a patient with HCDD. Our knock-in design allowed a conditional Cre-mediated deletion of the CH1 domain, reproducing the major event underlying the production of a pathogenic truncated HC. Beside the tissue deposition of the monoclonal human HC accurately reproducing the early events of the disease, this model also allowed exploration of the effect of the production of an isolated truncated monoclonal HC by plasma cells.

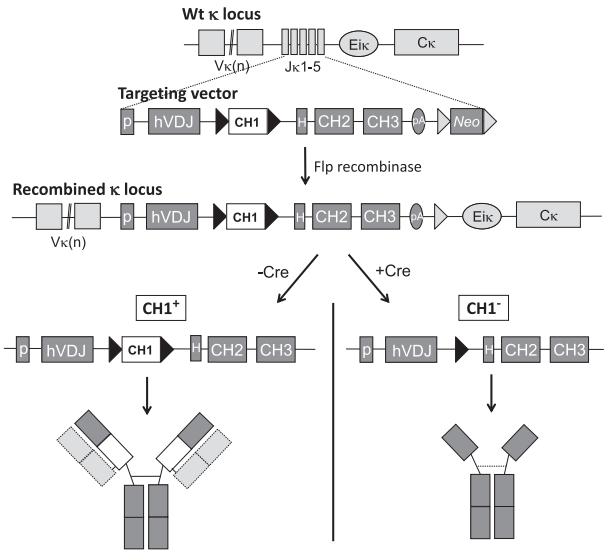

Figure 1. Structure of the targeted locus (not to scale). (Top) Representation of the WT unrearranged κ locus and the structure of the inserted human γHC gene replacing the Jκ region. (Middle) Resulting κ locus after targeted recombination is shown. The absence of Jκ segments precludes any Igκ LC rearrangement and expression. (Bottom) Cre-mediated deletion of the CH1 domain leads to the production of a truncated γ1HC as seen in the patient. In the absence of Cre-mediated deletion, a complete γHC is produced. Association with murine LCs is only depicted for the complete γHC (dashed boxes). The hypothetical disulfide bound between monomers of truncated γHC is also indicated (dashed line). Black triangles correspond to LoxP sites, and gray triangles are Frt sites.

Materials and methods

Mice

Gene targeting into the murine Igκ locus was performed as previously described.[36] Briefly, the gene coding the secreted form of a human monoclonal γ1HC extracted from a patient with HCDD was introduced in place of the mouse Jκ segments (Figure 1). The step-by-step procedure to reconstitute the complete human γHC, comprising a floxed *CH1* domain, is detailed in the supplemental Methods available on the *Blood* Web site, and primers are listed in supplemental Table 1. DH-LMP2A mice[37] were kindly provided by S. Casola (IFOM, Milan, Italy). All the protocols used were approved by our institutional review board for animal experimentation (Comité Régional d'Ethique de l'Expérimentation Animale du Limousin). Animals were maintained in pathogen-free conditions and analyzed at 6 months of age except when otherwise stated.

In vivo treatment, surgery, and biochemical parameters

Unilateral nephrectomy was performed on 8-week-old mice as previously described.[38] The removed kidneys were collected, and nephrectomized mice were euthanized 4 months later. Bortezomib (Velcade; Janssen Cilag) and cyclophosphamide (Endoxan; Baxter) (2 mg/kg) were injected subcutaneously at the indicated times. We used a bortezomib dose of 0.75 mg/kg per injection, which was previously shown to efficiently deplete plasma cells in another mouse model,[39] and which, in our hands, induced a >90% depletion of plasma cells at 24 hours. To test the sensitivity of plasma cells to bortezomib, we set up a protocol using 2 daily injections of a suboptimal dose (0.5 mg/kg) of bortezomib, leading to a depletion of ~70% of plasma cells in wild-type (WT) mice (supplemental Figure 1). Mice were euthanized for analysis 24 hours after the last injection. All injections were performed under anesthesia. Biochemical parameters were measured on overnight urine collections, and blood samples were obtained by retro-orbital puncture under anesthesia. Urine concentrations of creatinine and albumin were measured using the Creatinine Assay Kit (Abcam) and Albumin mouse enzyme-linked immunosorbent assay kit (Abcam), respectively, according to the manufacturer's recommendations.

Flow cytometry and cell sorting

Splenocytes were isolated and stained as previously described[40] with appropriate antibodies (supplemental Table 2). All the antibodies used to detect the human γHC were directed against the Fc part of immunoglobulin (Ig)G. Intracellular stainings were performed using the Intraprep kit (Beckman Coulter). Flow cytometry analyses were performed on a BD Pharmingen LSRFortessa cytometer, and cell sorting experiments were done using a BD FACSAria III cell sorter. Data were analyzed with BD FACSDiva software (BD Biosciences).

Pathologic studies

Kidney samples were processed for light microscopic examination, immunofluorescence, and electron microscopic studies, as previously described.[35,36] Briefly, immunofluorescence was performed on organs included in optimal cutting temperature compound and snap frozen in liquid nitrogen. Cryosections of 8 μm were fixed with cold acetone, blocked with phosphate-buffered saline (PBS) and 3% bovine serum albumin, and stained with appropriate antibodies (supplemental Table 2). Slides were observed on an LSM 510 confocal microscope (Zeiss). Immunoelectron microscopy was made on samples fixed with 4% glutaraldehyde in PBS and embedded in resin (TAAB Labs). Ultra-thin sections were processed for electron microscopy studies, incubated with anti–γ gold–conjugated,

and examined with a JEOL JEM-1010 electron microscope as previously described.[41] Toluidine blue-stained semithin sections were prepared and examined by light microscopy using a Zeiss Axioplan microscope (Zeiss) as previously described.[36] Description of scores of fluorescence intensity can be found in the supplemental Methods.

In vitro stimulations

Spleen B cells were magnetically enriched using the CD43 depletion kit (Miltenyi Biotec) according to the manufacturer's recommendations and stimulated in vitro (5×10^5 cell/mL) with 5 μg/mL lipopolysaccharide (LPS) (InVivoGen) for 4 days in RPMI supplemented with 10% fetal calf serum; 1×10^6 cells were used for flow cytometry analyzes, and the remaining cells were used for transcriptional analyzes.

Enzyme-linked immunosorbent assay

Serum were analyzed for the presence of human IgG (Fc), as previously described.[36] To reveal hybrid immunoglobulins composed of the human γHC associated with a murine κLC, we adapted the same protocol using coating with the anti-human IgG (Fc) and revelation with an anti-mouse κLC. For short-term HC production analysis, spleen cells or 3-day stimulated cells were counted, washed twice in PBS, normalized for the number of $CD138^+$ secreting cells, and plated in complete medium for 6 hours. Supernatants were collected and dosed by enzyme-linked immunosorbent assay. All antibodies used in the study are depicted in supplemental Table 2. Plates were read at 405 nm with a Xenius spectrophotometer (Safas).

Transcriptional analysis

Total RNA was extracted using TRI Reagent (Ambion). Reverse transcription was performed using the high-capacity cDNA reverse transcription kit (Applied Biosystems) on 3 μg of total RNA, with random hexamers. Relative quantification was performed with TaqMan Universal or SYBR Green Master Mix (Applied Biosystems) on cDNA samples (20 ng per reaction). Quantification of the gene of interest was analyzed by the ΔCt method with *Gapdh* used as the housekeeper gene. TaqMan probes for *Gapdh* (Mm99999915_g1), *CHOP* (Mm01135937_g1), *Herp* (Mm01249592_m1), and *BiP* (Mm01333324_g1) were used. For *Xbp1*, a polymerase chain reaction assay amplifying both the unspliced (u) and spliced (s) forms of *Xbp1* was performed. Ratios of *Xbp1s/Xbp1u* were calculated by scanning the blots and measuring the relative density of each band using ImageJ software. The *glyceraldehyde-3-phosphate dehydrogenase* gene was used as an internal loading control, and the primers are depicted in supplemental Table 1.

Statistical analysis

The statistical tests used to evaluate differences between variables were done using Prism GraphPad software (GraphPad Software). *P* values between variables were determined using the unpaired Student *t* test. $P < .05$ was considered significant.

Results

Generation and characterization of transgenic mice expressing complete and truncated human monoclonal γ1HC

A genetically reconstituted gene encoding the *VDJ* sequence from a patient with HCDD associated with the complete secreted form of the human *γ1* constant region was inserted in the murine κ locus to force expression of the human γ1HC throughout B-cell differentiation ($CH1^+$ mice). To generate a truncated γHC similar to that extracted from the patient, we flanked the CH1 sequence with 2 loxP sites, allowing its Cre-mediated deletion ($CH1^-$ mice) (Figure 1; supplemental Figure 2A). About half of the $CH1^+$ and $CH1^-$ plasma cells were shown to express the human γHC together with a murine immunoglobulin (Figure 2A; supplemental Figure 2B). We further crossed these mice with the DH-LMP2A mice in which the HC locus was invalidated by the targeted insertion of the Epstein-Barr virus protein LMP2A that mimics B-cell receptor signaling and allows complete B-cell development.[37] We recently showed that DH-LMP2A mice feature increased plasma cell differentiation despite the absence of endogenous HCs.[40] Consequently, $DH\text{-}CH1^-$ and $DH\text{-}CH1^+$ mice closely recapitulate the features of a monoclonal gammopathy with an elevated number of plasma cells producing the human monoclonal γHC in the absence of endogenous murine HC (Figure 2B). Of note, the percentage of plasma cells is equivalent in all DH strains (Figure 2B), and only about 50% of plasma cells coexpressed a murine κLC (supplemental Figure 2B). In sera, human γHC rates were more elevated in $CH1^+$ than in $DH\text{-}CH1^+$ mice [5830 ± 452 μg/mL (mean ± standard error of the meain [SEM]) vs 2949 ± 451 μg/mL, respectively; Figure 2B). This result may be related to the absence of endogenous LCs in ~50% of plasma cells in DH mice (supplemental Figure 2B) that likely precludes the secretion of the isolated HC due to intracellular retention by the chaperone protein BiP.[20,42,43] Cre-mediated deletion of the CH1 domain resulted in the production of the expected truncated human γ1HC (supplemental Figure 2A). Strikingly, this deletion was associated with a massive decrease of serum human γHCs in both $CH1^-$ (24.73 ± 1.1 μg/mL) and $DH\text{-}CH1^-$ mice (34.88 ± 8.8 μg/mL) (Figure 2B), which was partially due to a defective secretion by plasma cells as observed by dosage of human γHCs in supernatants of 6-hour cultures of either spleen cells or 3-day LPS-stimulated B cells (Figure 2C). We detected only traces of human γHC in urines in both $CH1^+$ and $CH1^-$ mice (supplemental Figure 2C), showing that the low level in sera is not due to an increased renal excretion. Similarly to previous observations,[11,20] we readily detected hybrid immunoglobulins composed of the truncated human γHC associated with a murine LC (supplemental Figure 2D). However, in the absence of available standards, it remained difficult to precisely evaluate the proportion of these noncovalently linked HC/LC immunoglobulins compared with free HC.

Truncated human γHC recapitulates the renal lesions of HCDD in mouse

We further carried out pathologic studies of kidney sections from 6-month-old mice. Despite the low serum level of human-truncated γ1HCs in mice, immunofluorescence studies revealed typical linear HC deposits along the glomerular, vascular, and tubular BMs in $CH1^-$ (supplemental Figure 3A) and $DH\text{-}CH1^-$ kidneys (Figure 3A). These deposits were more pronounced in $DH\text{-}CH1^-$ than in $CH1^-$ kidneys (scores = 3.6 ± 0.19 [mean ± SEM] vs 1.75 ± 0.48, respectively; Figure 3B) and were not stained with anti-mouse κLC (supplemental Figure 3A). Linear vascular γ1HC deposits were also observed in lung and liver (supplemental Figure 3B). Immunoglobulin deposits were not observed in WT, DH, or $DH\text{-}CH1^+$ kidneys, demonstrating the specific pathogenicity of the truncated HC (Figure 3A-B). Discrete nonlinear deposits were observed in some $CH1^+$ glomeruli, likely related to immune complexes deposits because they partially colocalized with murine κLC (supplemental Figure 3A) and were absent in $DH\text{-}CH1^+$ mice that lack murine immunoglobulin. Antibodies specific for human γHC domains confirmed the absence of the CH1 domain in deposits, whereas similar staining patterns were observed with the anti-γCH2 and anti-human IgG conjugates (supplemental Figure 3C). Due to higher deposit scores, further studies were carried out in $DH\text{-}CH1^-$ mice and compared with DH mice as control, except when indicated. Linear glomerular and peritubular γ1HC deposits were detectable in kidneys of 2-month-old mice and increased up to 6 months (supplemental Figure 3D). We did not observe a significant increase in renal deposits either in 12- (supplemental Figure 3D) and 18-month-old mice (not

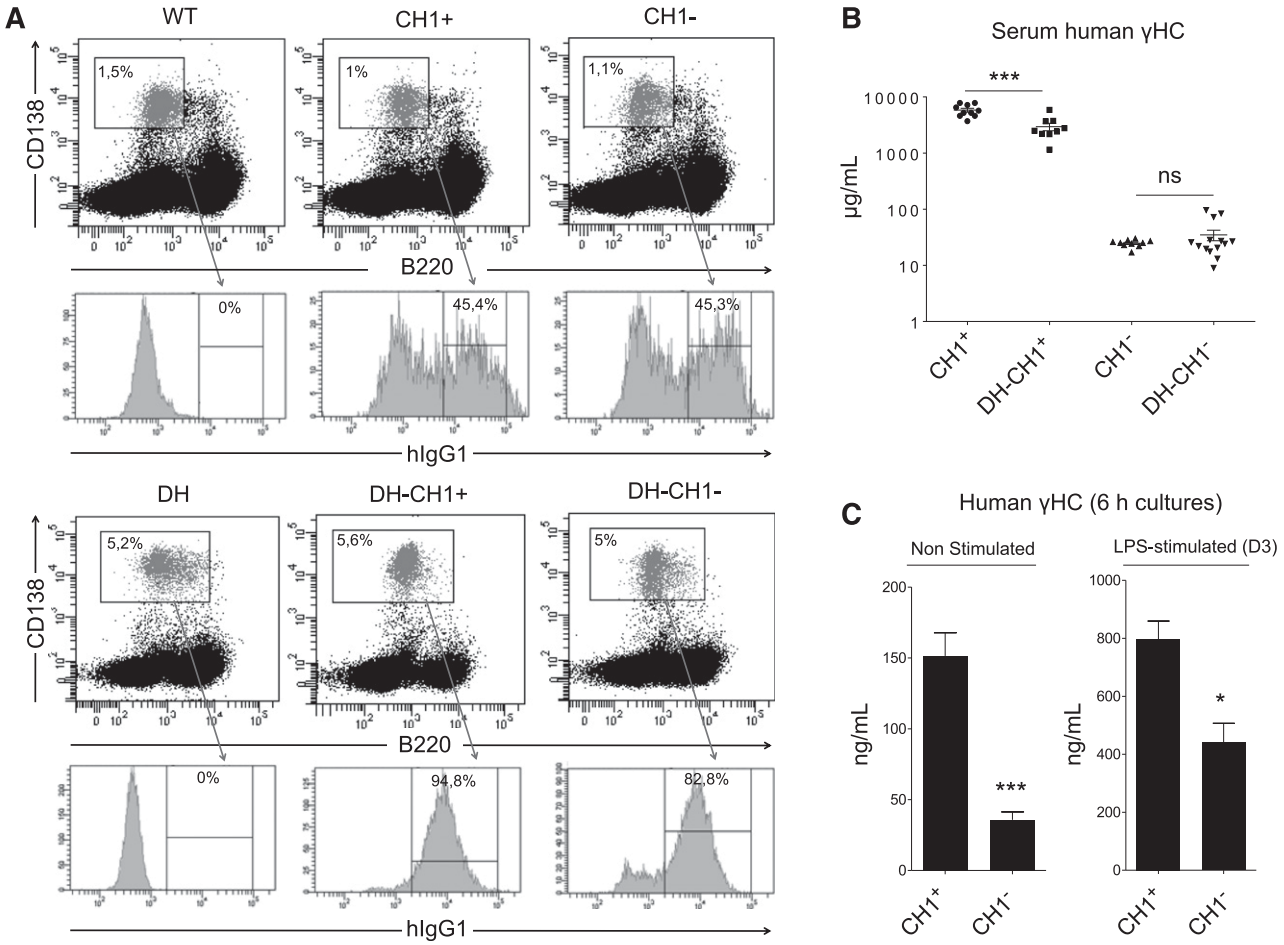

Figure 2. Characterization of the murine model of HCDD. (A) Splenocytes from 6-month-old WT, CH1$^+$, or CH1$^-$ (top) and DH, DH-CH1$^+$, or DH-CH1$^-$ (bottom) mice were stained with the indicated antibodies and analyzed by flow cytometry. Representative results from 3 independent experiments with ≥2 mice of each strain are shown. Numbers indicate percentages of plasma cells on biparametric graphs and human γHC-positive plasma cells on histograms. (B) Serum human γHC production from 8- to 12-week-old mice. Each dot represents an individual mouse. Results are expressed in log scale as mean ± SEM (µg/mL; n = 9-14 per group in ≥3 independent experiments; ns, not significant; ***$P < .001$). (C) Human γHC production in supernatants of 6-hour cultures of nonstimulated spleen cells (left) and 3-day LPS stimulated B cells (right). Plated cell counts were normalized on the number of secreting CD138$^+$ cells. Means ± SEM (ng/mL) are shown (n = 4 per strain in 2 independent experiments; *$P < .05$; ***$P < .001$).

shown) or in mice unilaterally nephrectomized at 2 months of age and euthanized 4 months later (supplemental Figure 3D). Immunoelectron microscopy studies confirmed the presence of nonorganized linear deposits along tubular and glomerular BMs, which stained with the anti-human γHC gold-labeled antibody, similar to those observed in the patient's kidney biopsy samples (Figure 3C-D). Finally, toluidine blue staining revealed a faint diffuse thickening of medullary tubular and glomerular BMs, as well as in the mesangium, with no evidence of nodular glomerulosclerosis (Figure 3E), even in 18-month-old mice or unilaterally nephrectomized mice (data not shown).

HCDD mice show early signs of glomerulosclerosis but no renal dysfunction

The increased production by mesangial cells of ECM proteins including laminin, collagen type IV, fibronectin, and, more specifically, tenascin-C is a hallmark of early glomerular changes in LCDD.[25,28] We therefore investigated the potential glomerular accumulation of tenascin-C in DH-CH1$^-$ kidneys. Immunofluorescence studies revealed a significant ($P = .0002$) increase in tenascin-C in DH-CH1$^-$ compared with control DH kidneys (scores = 2.11 ± 0.22 vs 0.67 ± 0.11; mean ± SEM; Figure 4A; supplemental Figure 3D). Because HCDD usually manifests with glomerular proteinuria, we compared the urine albumin/creatinine ratio of DH and DH-CH1$^-$ mice. We observed no significant difference despite a trend toward the increase in DH-CH1$^-$ mice compared with DH mice (8560 ± 1575 vs 22 330 ± 8283; mean ± SEM; Figure 4B).

Inhibition of kidney HC deposits on hematologic treatment

To validate the usefulness of our MIDD model for therapeutic investigations, we treated 5-month-old CH1$^-$ mice for 5 weeks using 2 injections of cyclophosphamide followed by repeated injections of bortezomib (Figure 5A), with the aim of reducing the production of the pathogenic human γHC. This treatment was inspired by the CyBorD (cyclophosphamide, bortezomib, dexamethasone) combination, which is widely used in the various disorders associated with monoclonal gammopathies.[5,44-47] Cyclophosphamide was shown to efficiently deplete B cells and to lower serum human γHC (supplemental Figure 4A-B), and further repeated additions of bortezomib maintained a low level of human γHC compared with nontreated mice (supplemental Figure 4B). After 5 weeks of treatment, animals were euthainzed and analyzed for kidney deposits. We observed a significant inhibition of HC deposits in kidneys of treated mice compared with nontreated mice (scores = 2.214 ± 0.3058 vs 0.8333 ± 0.2472; mean ± SEM; $P = .0056$; Figure 5B). Although incomplete, recovery of kidney lesions correlated with partial hematologic response, as illustrated by persistence of detectable low serum level of human γHC (supplemental Figure 4B).

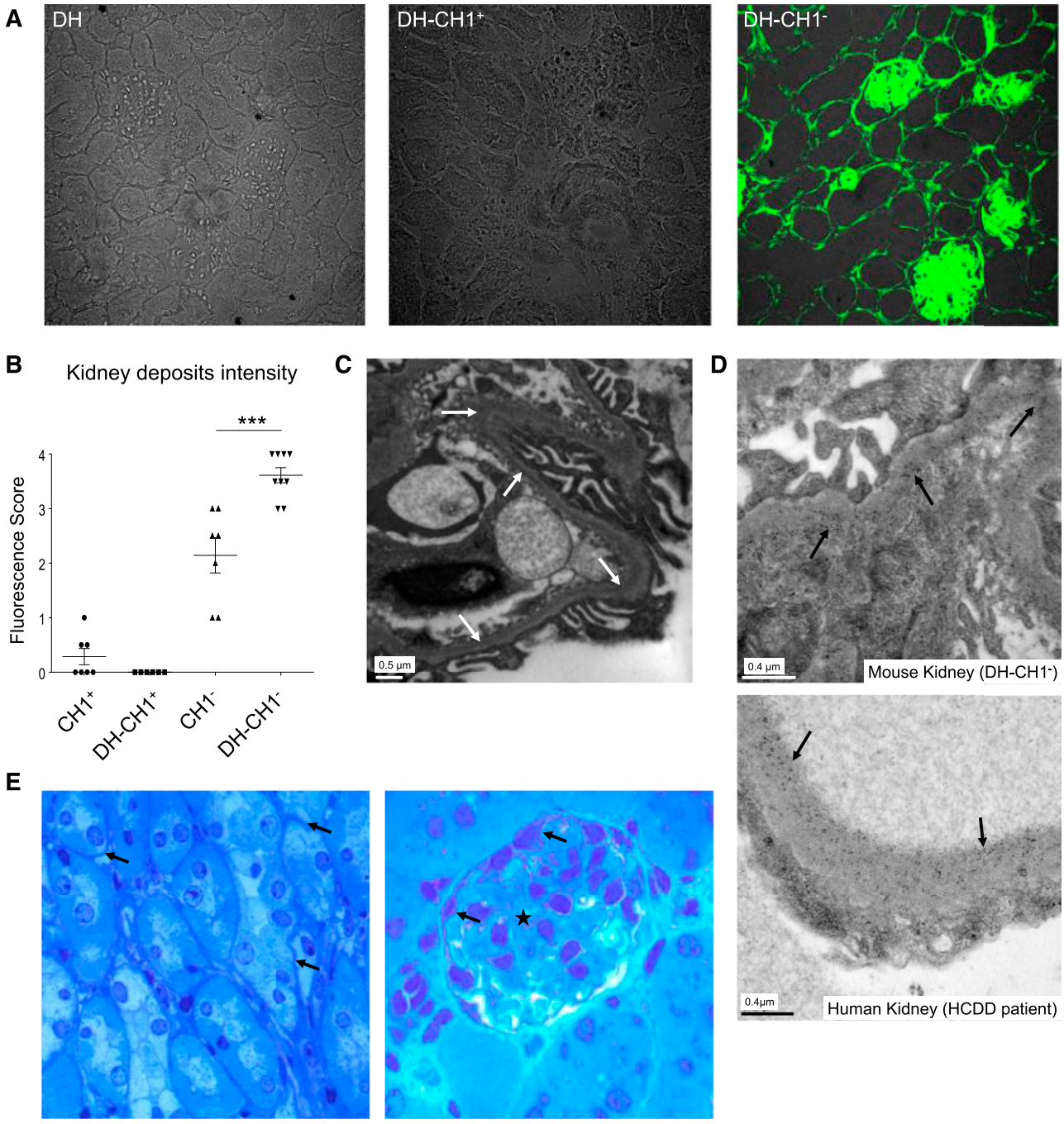

Figure 3. HCDD transgenic mice reproduce human kidney lesions. (A) Immunofluorescence microscopy on DH, DH-CH1$^+$, or DH-CH1$^-$ kidney sections with an anti-human γHC-fluorescein isothiocyanate. Fluorescence and differential interference contrast are merged. Original magnification, ×400. Note the intense linear staining of tubular and glomerular BMs and in the mesangium of the DH-CH1$^-$ kidney. (B) Deposit intensity based on immunofluorescence studies of kidney sections. Each dot represents a score of fluorescence from an individual kidney as described in Materials and Methods. Means ± SEM are shown (n = 6-9 mice in 3 independent experiments; ***$P < .001$). (C) Electron micrograph of kidney from a DH-CH1$^-$ mouse showing finely granular electron-dense deposits along the inner part of the lamina densa of a glomerular-capillary BMs (arrows). Original magnification, ×20 000; scale bar is indicated. (D) Immunoelectron microscopy on kidney from a DH-CH1$^-$ mouse (top) and a renal biopsy of the corresponding HCDD patient (bottom). Note the presence of anti–γHC-conjugated gold particles along the BMs in both patient and mice kidneys. Original magnification, ×50 000; scale bars are indicated. (E) Toluidine blue staining showing a faint diffuse thickening of tubular BMs in the outer medulla (left) and glomerular BMs (arrows). Deposits are also observed in the mesangium (star). Original magnification, ×600.

Truncated γHC-producing plasma cells display exacerbated ER stress and are highly sensitive to proteasome inhibition

Several recent case reports have highlighted the efficiency of bortezomib-based treatments in HCDD.[5,48] We then sought to determine whether the production of an isolated truncated γHC could influence the fate of plasma cells on proteasome inhibitor treatment. Spleen plasma cell count was performed in WT, DH, and DH-CH1$^-$ mice after 2 daily injections of bortezomib (0.5 mg/kg) and compared with nontreated mice from the corresponding strains. At posttreatment day 3, we observed a more efficient depletion of plasma cells in DH-CH1$^-$ than in WT or DH mice (Figure 6A-B; supplemental Figure 5). We then hypothesized that the increased effect of bortezomib could be related to an exacerbated ER stress induced by the production of an isolated truncated γHC.

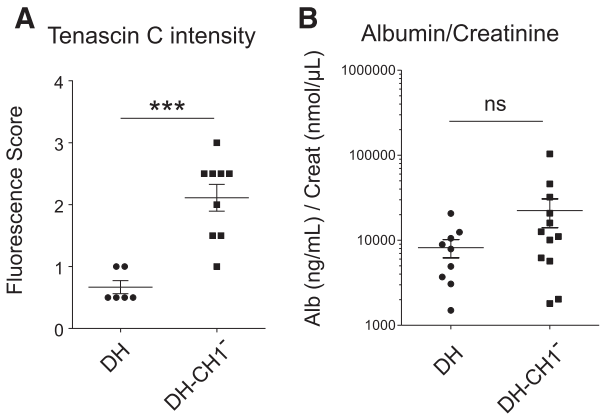

Figure 4. Tenascin-C accumulation and kidney function. (A) Comparison of tenascin-C accumulation in glomeruli by immunofluorescence studies of kidney sections. Each dot represents the score of fluorescence from an individual kidney. Means ± SEM are shown (n = 6-9 mice in 3 independent experiments; ***$P < .001$). (B) Urine albumin to creatinine ratio was measured on overnight urine samples from DH and DH-CH1$^-$ mice. Each dot represents the result from an individual mouse. Values are indicated in ng/mL (albumin) per nmol/µL (creatinine). Means ± SEM are shown (n = 9-12 mice; ns, not significant).

We analyzed the transcriptional expression of ER stress markers *Chop*, *BiP/GRP78*, *HERP*, and *Xbp1s* in 4-day LPS-stimulated B cells, a condition known to induce differentiation toward secreting plasmablasts.[40] As previously described,[40] we observed an increased plasmablast differentiation in DH mice compared with WT but also with DH-CH1$^-$ mice (supplemental Figure 6A-B). These differences seem to be due to an intrinsic higher propensity to terminal differentiation of DH cells and not to an increased apoptosis of WT and DH-CH1$^-$ cells during LPS stimulation (supplemental Figure 6C). Compared with WT cells that produce complete immunoglobulins, or DH cells producing either no immunoglobulin or isolated LCs (supplemental Figure 2B), we observed a significant increase in several ER stress markers in stimulated B cells of DH-CH1$^-$ mice (Figure 6C-D), including *BiP*, *Xbp1s*, or the proapoptotic transcription factor *Chop* known to be repressed during normal plasma cell differentiation.[49] The increase in *Xbp1s* and *Chop* was further confirmed in sorted plasma cells of DH-CH1$^-$ mice compared with WT or DH mice (Figure 6C-D). No significant difference was detected in WT vs DH mice either in sorted plasma cells or in stimulated B cells.

Discussion

We characterized the first transgenic murine model of human MIDD. Using an established strategy of gene targeting in the κ locus,[36] we introduced a sequence coding a human γ1HC from a patient with Randall-type HCDD. HCDD is characterized by tissue deposition, mostly in the kidney, of an isolated truncated monoclonal HC that lacks the CH1 domain but invariably displays a complete VH domain. Then, we analyzed mice producing an artificially reconstituted complete human γ1HC comprising the CH1 domain and its CH1-truncated counterpart. We demonstrated that mice secreting full-length γHC, which efficiently associates with murine LCs, did not show any evidence of glomerular and tubular lesions. By contrast, deletion of the CH1 domain led to the progressive appearance of the hallmark renal pathologic changes in HCDD, eg, amorphous linear deposits of the isolated γHC along tubular and glomerular BMs and in the mesangium. The absence of glomerular proteinuria and glomerulosclerosis, 2 frequent features of HCDD, was probably related the mixed genetic background of the transgenic mice because both *C57BL/6* and *129/Sv* mice were shown to be highly resistant in models of nephron reduction or diabetic nephropathy.[50-52] Whether backcrossing of our HCDD mouse model to nephropathy-prone genetic background like DBA/2J could overcome this issue remains to be confirmed.[51] Nevertheless, γHC deposits were accompanied by glomerular accumulation of tenascin-C, a typical marker of ECM remodeling that precedes development of nodular glomeruloscerosis in LCDD.[28] Consequently, our model remains relevant to accurately study in vivo the early phenotypic modifications of mesangial cells (induction of transforming growth factor β, matrix metalloproteinase 7 activity, etc)[25,27-29] and to test new therapeutic approaches to prevent glomerular injury in MIDD.

It was previously demonstrated that the ER resident chaperone protein BiP/GRP78 retains free HC by stable interaction with the CH1 domain, until a LC displaces this association and allows secretion of an entire immunoglobulin.[42] Monoclonal γHC lacking the CH1 domain was consequently supposed to be freely secreted by plasma cells.[20-22] Accordingly, isolated HCs produced by plasma cells in human diseases

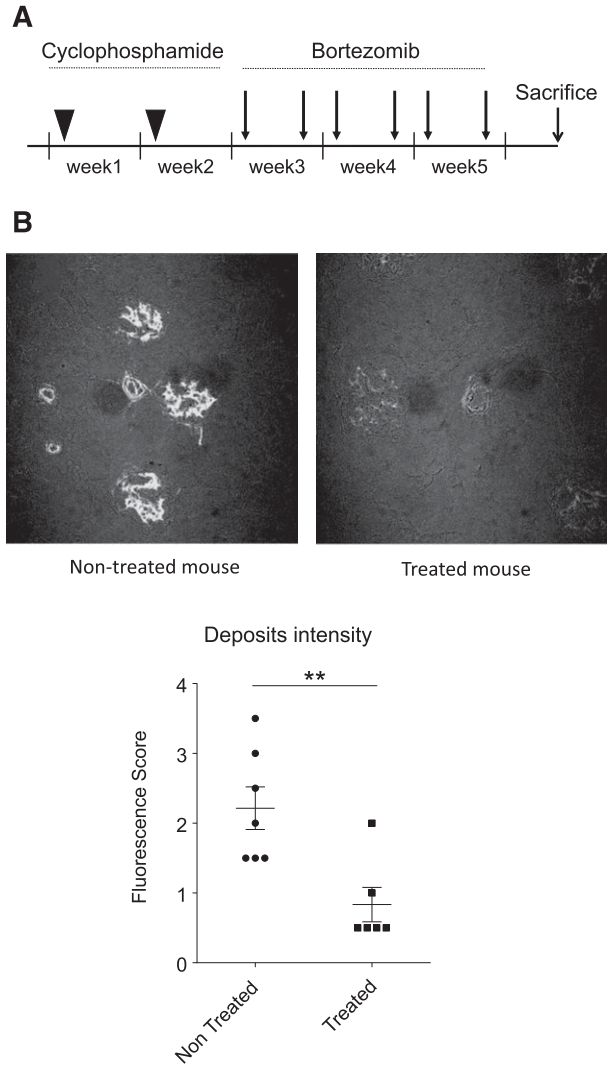

Figure 5. Hematologic treatment reduces the onset of kidney deposits. (A) Therapeutic protocol applied to deplete B and plasma cells in CH1$^-$ mice. (B) (Upper) Representative immunofluorescence on kidney sections of treated or nontreated CH1$^-$ mice with an anti-human γHC-fluorescein isothiocyanate. Original magnification, ×400. (Lower) Comparison of deposit intensity in kidney sections of treated vs nontreated CH1$^-$ mice. Each dot represents the score of fluorescence from an individual kidney. Means ± SEM are shown (n = 6-7 mice in 2 independent experiments; **$P < .01$).

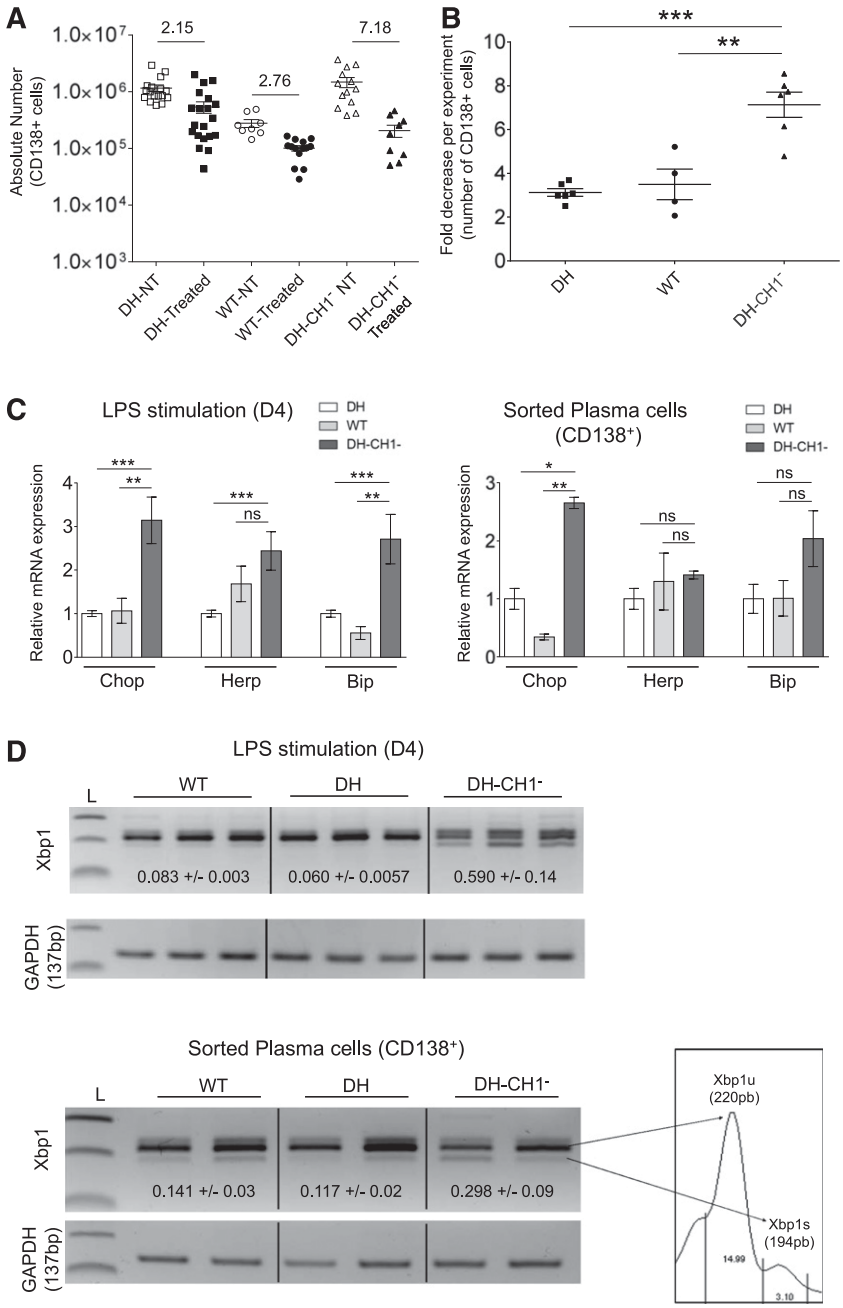

Figure 6. Plasma cells producing a truncated γHC are highly sensitive to bortezomib. (A) Absolute number of spleen plasma cells in nontreated and bortezomib-treated mice. Each dot represents a mouse and numbers indicate the overall means of fold decrease in each strain (n = 8-17 mice). (B) Fold decrease of spleen plasma cells on 48 hours of bortezomib treatment. Each dot represents the fold decrease of plasma cell number ($CD138^+/B220^{low}$ cells) in an independent experiment with ≥2 treated and 2 nontreated mice. Means ± SEM are shown (n = 4-6 independent experiments; $^{**}P < .01$; $^{***}P < .001$). (C) Quantitative transcriptional analysis of ER stress markers in (left) 4-day LPS-stimulated B cells and (right) sorted $CD138^+$ spleen plasma cells from DH (white bars), WT (light gray bars), and DH-$CH1^-$ (dark gray bars) mice. Results are means ± SEM of 3 independent experiments with (B) 2 mice of each strain and (C) 2 experiments of sorted plasma cells. ns, not significant; $^{*}P < .05$; $^{**}P < .01$; $^{***}P < .001$). (D) Gel electrophoresis of reverse transcriptase-polymerase chain reaction detecting full-length unspliced (u) and spliced (s) forms of *Xbp1* in 4-day (upper) LPS-stimulated B cells and (lower) sorted $CD138^+$ spleen plasma cells from WT, DH, or DH-$CH1^-$ mice. Numbers indicate the ratios of *Xbp1s/Xbp1u*. (Lower right) An example of quantification of band intensities is shown. The upper unspecific band was excluded from the calculation. *Glyceraldehyde-3-phosphate dehydrogenase* was used as a loading control. L, 100-bp ladder.

(HC disease and HCDD) are invariably characterized by the absence of the CH1 domain. However, in our model, the deletion of the CH1 domain led to a massive decrease of circulating γHC, partially due to a defective secretion by plasma cells. Whether a defective interaction between CH1-truncated γHCs and the neonatal Fc receptor (FcRn), known to protect IgG from degradation, could further explain this result remains to be explored.[53] As previously hypothesized, another nonexclusive possibility could be related to the high avidity for BMs of truncated HCs.[11,54] In any case, this observation correlates with the low serum level of monoclonal HC usually observed in HCDD patients, making difficult both diagnostic assessment and evaluation of treatment efficacy in this disease.[31] It also demonstrates the striking nephrotoxic effect of circulating truncated HCs featuring an entire V domain.

Finally, our model showed that plasma cells producing a truncated γHC are more sensitive to bortezomib treatment than their WT counterpart producing complete immunoglobulins. Accumulating evidence has linked protein synthesis to the responsiveness of proteasome inhibitors in multiple myeloma.[55-58] Moreover, proteasome inhibitors were shown to trigger the protein kinase RNA-like endoplasmic reticulum kinase-dependent branch of the unfolded protein response and CHOP, leading to a terminal ER stress response due to accumulation of unfolded proteins.[57-59] Here, we demonstrated that isolated truncated γHCs are poorly secreted by plasma cells, which in turn, are intrinsically and basically stressed as observed by overexpression of CHOP and XBP1s. We then hypothesize that truncated γHCs, due to their incomplete assembly[11,20] and/or their high propensity to aggregate, may represent exquisite substrates to trigger ER stress, lowering the threshold for terminal unfolded protein response on proteasome inhibitor treatments.[58] This could explain the efficacy of bortezomib-based regimens in HCDD.[5,48] Further investigations should be conducted to accurately decipher the mechanisms leading

to ER stress in plasma cells producing truncated HCs. In a broader view, the intrinsic toxicity for plasma cells of immunoglobulin fragments prone to misfolding and aggregation deserves to be explored in other monoclonal immunoglobulin-related diseases including light chain (AL) amyloidosis and LCDD, in which preliminary studies suggest that bortezomib-based therapy has a strong impact on renal and patient outcomes.[44,60-62] Transgenic mouse models could be of invaluable interest to explore this issue.[36]

Altogether, the present transgenic mouse model of HCDD accurately recapitulates the early steps of the human pathology and represents a valuable tool to explore the mechanisms that govern toxicity of truncated HCs and the sequential events leading to glomerular injury in MIDD. It also raises new perspectives to test innovative therapeutic approaches.

Acknowledgments

The authors thank the staff of the animal facility, the cell cytometry facility of Limoges, J. M. Goujon at the Department of Pathology of Poitiers, M. Clavel, S. Lecardeur, and C. Carrion for technical assistance, Benoît Marin for help in statistical analyses, and A. Jaccard for helpful discussion. This work was supported by grants from Fondation pour la Recherche Médicale, Association pour la Recherche sur le Cancer (grant SL220100601332), Institut Universitaire de France, Région Limousin, and Fondation Française pour la Recherche contre le Myelome et les Gammapathies monoclonales. A.B. and N.S. were funded by fellowships from the Ligue National Contre le Cancer, Région Limousin, and the French Ministry of Research.

Authorship

Contribution: A.B. and S.B. designed, performed, and analyzed experiments and drafted the manuscript; C.L., N.S., C.O., A.D., N.Q., and V.J. performed experiments and analyzed data; L.D., M.C., and G.T. provided general advice and critically reviewed the manuscript; F.B. provided general advice and wrote the manuscript; and C.S. designed and supervised research and wrote the manuscript.

Conflict-of-interest disclosure: The authors declare no competing financial interests.

Correspondence: Christophe Sirac, CRIBL laboratory, CNRS UMR7276, CBRS room 110, 2 rue du Dr Marcland, 87000 Limoges, France; e-mail: christophe.sirac@unilim.fr.

References

1. Merlini G, Stone MJ. Dangerous small B-cell clones. *Blood.* 2006;108(8):2520-2530.
2. Leung N, Bridoux F, Hutchison CA, et al; International Kidney and Monoclonal Gammopathy Research Group. Monoclonal gammopathy of renal significance: when MGUS is no longer undetermined or insignificant. *Blood.* 2012;120(22):4292-4295.
3. Buxbaum J, Gallo G. Nonamyloidotic monoclonal immunoglobulin deposition disease. Light-chain, heavy-chain, and light- and heavy-chain deposition diseases. *Hematol Oncol Clin North Am.* 1999;13(6):1235-1248.
4. Lin J, Markowitz GS, Valeri AM, et al. Renal monoclonal immunoglobulin deposition disease: the disease spectrum. *J Am Soc Nephrol.* 2001; 12(7):1482-1492.
5. Nasr SH, Valeri AM, Cornell LD, et al. Renal monoclonal immunoglobulin deposition disease: a report of 64 patients from a single institution. *Clin J Am Soc Nephrol.* 2012;7(2):231-239.
6. Bridoux F, Leung N, Hutchison CA, et al; International Kidney and Monoclonal Gammopathy Research Group. Diagnosis of monoclonal gammopathy of renal significance. *Kidney Int.* 2015;87(4):698-711.
7. Preud'homme JL, Aucouturier P, Touchard G, et al. Monoclonal immunoglobulin deposition disease: a review of immunoglobulin chain alterations. *Int J Immunopharmacol.* 1994;16(5-6): 425-431.
8. Aucouturier P, Khamlichi AA, Touchard G, et al. Brief report: heavy-chain deposition disease. *N Engl J Med.* 1993;329(19):1389-1393.
9. Khamlichi AA, Aucouturier P, Preud'homme JL, Cogné M. Structure of abnormal heavy chains in human heavy-chain-deposition disease. *Eur J Biochem.* 1995;229(1):54-60.
10. Tubbs RR, Berkley V, Valenzuela R, et al. Pseudo-gamma heavy chain (IgG4 lambda) deposition disease. *Mod Pathol.* 1992;5(2): 185-190.
11. Moulin B, Deret S, Mariette X, et al. Nodular glomerulosclerosis with deposition of monoclonal immunoglobulin heavy chains lacking C(H)1. *J Am Soc Nephrol.* 1999;10(3):519-528.
12. Denoroy L, Déret S, Aucouturier P. Overrepresentation of the V kappa IV subgroup in light chain deposition disease. *Immunol Lett.* 1994;42(1-2):63-66.
13. Déret S, Chomilier J, Huang DB, Preud'homme JL, Stevens FJ, Aucouturier P. Molecular modeling of immunoglobulin light chains implicates hydrophobic residues in non-amyloid light chain deposition disease. *Protein Eng.* 1997; 10(10):1191-1197.
14. Rocca A, Khamlichi AA, Aucouturier P, et al. Primary structure of a variable region of the V kappa I subgroup (ISE) in light chain deposition disease. *Clin Exp Immunol.* 1993;91(3):506-509.
15. Decourt C, Cogné M, Rocca A. Structural peculiarities of a truncated V kappa III immunoglobulin light chain in myeloma with light chain deposition disease. *Clin Exp Immunol.* 1996;106(2):357-361.
16. Decourt C, Touchard G, Preud'homme J-L, et al. Complete primary sequences of two λ immunoglobulin light chains in myelomas with nonamyloid (Randall-type) light chain deposition disease. *Am J Pathol.* 1998;153(1):313-318.
17. Kaplan B, Livneh A, Gallo G. Charge differences between in vivo deposits in immunoglobulin light chain amyloidosis and non-amyloid light chain deposition disease. *Br J Haematol.* 2007;136(5): 723-728.
18. Kaplan B, Ramirez-Alvarado M, Dispenzieri A, et al. Isolation and biochemical characterization of plasma monoclonal free light chains in amyloidosis and multiple myeloma: a pilot study of intact and truncated forms of light chains and their charge properties. *Clin Chem Lab Med.* 2008; 46(3):335-341.
19. Soma J, Sato K, Sakuma T, et al. Immunoglobulin gamma3-heavy-chain deposition disease: report of a case and relationship with hypocomplementemia. *Am J Kidney Dis.* 2004; 43(1):E10-E16.
20. Hendershot L, Bole D, Köhler G, Kearney JF. Assembly and secretion of heavy chains that do not associate posttranslationally with immunoglobulin heavy chain-binding protein. *J Cell Biol.* 1987;104(3):761-767.
21. Zou X, Osborn MJ, Bolland DJ, et al. Heavy chain-only antibodies are spontaneously produced in light chain-deficient mice. *J Exp Med.* 2007; 204(13):3271-3283.
22. Feige MJ, Hendershot LM, Buchner J. How antibodies fold. *Trends Biochem Sci.* 2010;35(4): 189-198.
23. Cogné M, Silvain C, Khamlichi AA, Preud'homme JL. Structurally abnormal immunoglobulins in human immunoproliferative disorders. *Blood.* 1992;79(9):2181-2195.
24. Herrera GA, Shultz JJ, Soong SJ, Sanders PW. Growth factors in monoclonal light-chain–related renal diseases. *Hum Pathol.* 1994;25(9):883-892.
25. Zhu L, Herrera GA, Murphy-Ullrich JE, Huang ZQ, Sanders PW. Pathogenesis of glomerulosclerosis in light chain deposition disease. Role for transforming growth factor-beta. *Am J Pathol.* 1995;147(2):375-385.
26. Keeling J, Teng J, Herrera GA. AL-amyloidosis and light-chain deposition disease light chains induce divergent phenotypic transformations of human mesangial cells. *Lab Invest.* 2004;84(10): 1322-1338.
27. Keeling J, Herrera GA. Matrix metalloproteinases and mesangial remodeling in light chain-related glomerular damage. *Kidney Int.* 2005;68(4): 1590-1603.
28. Keeling J, Herrera GA. An in vitro model of light chain deposition disease. *Kidney Int.* 2009;75(6): 634-645.
29. Russell WJ, Cardelli J, Harris E, Baier RJ, Herrera GA. Monoclonal light chain–mesangial cell interactions: early signaling events and subsequent pathologic effects. *Lab Invest.* 2001; 81(5):689-703.
30. Ronco P, Plaisier E, Aucouturier P. Monoclonal immunoglobulin light and heavy chain deposition diseases: molecular models of common renal diseases. *Contrib Nephrol.* 2011;169:221-231.
31. Ronco P, Plaisier E, Mougenot B, Aucouturier P. Immunoglobulin light (heavy)-chain deposition disease: from molecular medicine to pathophysiology-driven therapy. *Clin J Am Soc Nephrol.* 2006;1(6):1342-1350.

32. Yang CW, Hattori M, Vlassara H, et al. Overexpression of transforming growth factor-beta 1 mRNA is associated with up-regulation of glomerular tenascin and laminin gene expression in nonobese diabetic mice. *J Am Soc Nephrol.* 1995;5(8):1610-1617.

33. Herrera GA, Russell WJ, Isaac J, et al. Glomerulopathic light chain-mesangial cell interactions modulate in vitro extracellular matrix remodeling and reproduce mesangiopathic findings documented in vivo. *Ultrastruct Pathol.* 1999;23(2):107-126.

34. Khamlichi AA, Rocca A, Touchard G, Aucouturier P, Preud'homme JL, Cogné M. Role of light chain variable region in myeloma with light chain deposition disease: evidence from an experimental model. *Blood.* 1995;86(10): 3655-3659.

35. Decourt C, Rocca A, Bridoux F, et al. Mutational analysis in murine models for myeloma-associated Fanconi's syndrome or cast myeloma nephropathy. *Blood.* 1999;94(10):3559-3566.

36. Sirac C, Bridoux F, Carrion C, et al. Role of the monoclonal kappa chain V domain and reversibility of renal damage in a transgenic model of acquired Fanconi syndrome. *Blood.* 2006; 108(2):536-543.

37. Casola S, Otipoby KL, Alimzhanov M, et al. B cell receptor signal strength determines B cell fate. *Nat Immunol.* 2004;5(3):317-327.

38. Mallipattu SK, Gallagher EJ, LeRoith D, et al. Diabetic nephropathy in a nonobese mouse model of type 2 diabetes mellitus. *Am J Physiol Renal Physiol.* 2014;306(9):F1008-F1017.

39. Neubert K, Meister S, Moser K, et al. The proteasome inhibitor bortezomib depletes plasma cells and protects mice with lupus-like disease from nephritis. *Nat Med.* 2008;14(7):748-755.

40. Lechouane F, Bonaud A, Delpy L, et al. B-cell receptor signal strength influences terminal differentiation. *Eur J Immunol.* 2013;43(3): 619-628.

41. Bridoux F, Sirac C, Hugue V, et al. Fanconi's syndrome induced by a monoclonal Vkappa3 light chain in Waldenstrom's macroglobulinemia. *Am J Kidney Dis.* 2005;45(4):749-757.

42. Hendershot LM. Immunoglobulin heavy chain and binding protein complexes are dissociated in vivo by light chain addition. *J Cell Biol.* 1990;111(3): 829-837.

43. Haas IG, Wabl M. Immunoglobulin heavy chain binding protein. *Nature.* 1983;306(5941):387-389.

44. Venner CP, Lane T, Foard D, et al. Cyclophosphamide, bortezomib, and dexamethasone therapy in AL amyloidosis is associated with high clonal response rates and prolonged progression-free survival. *Blood.* 2012; 119(19):4387-4390.

45. Mikhael JR, Schuster SR, Jimenez-Zepeda VH, et al. Cyclophosphamide-bortezomib-dexamethasone (CyBorD) produces rapid and complete hematologic response in patients with AL amyloidosis. *Blood.* 2012;119(19):4391-4394.

46. Shah G, Kaul E, Fallo S, et al. Bortezomib subcutaneous injection in combination regimens for myeloma or systemic light-chain amyloidosis: a retrospective chart review of response rates and toxicity in newly diagnosed patients. *Clin Ther.* 2013;35(10):1614-1620.

47. Kikukawa Y, Yuki H, Hirata S, et al. Combined use of bortezomib, cyclophosphamide, and dexamethasone induces favorable hematological and organ responses in Japanese patients with amyloid light-chain amyloidosis: a single-institution retrospective study. *Int J Hematol.* 2015;101(2):133-139.

48. Patel K, Dillon JJ, Leung N, et al. Use of bortezomib in heavy-chain deposition disease: a report of 3 cases. *Am J Kidney Dis.* 2014;64(1): 123-127.

49. Ma Y, Shimizu Y, Mann MJ, Jin Y, Hendershot LM. Plasma cell differentiation initiates a limited ER stress response by specifically suppressing the PERK-dependent branch of the unfolded protein response. *Cell Stress Chaperones.* 2010; 15(3):281-293.

50. Zheng F, Striker GE, Esposito C, Lupia E, Striker LJ. Strain differences rather than hyperglycemia determine the severity of glomerulosclerosis in mice. *Kidney Int.* 1998;54(6):1999-2007.

51. Qi Z, Fujita H, Jin J, et al. Characterization of susceptibility of inbred mouse strains to diabetic nephropathy. *Diabetes.* 2005;54(9):2628-2637.

52. Ma L-J, Fogo AB. Model of robust induction of glomerulosclerosis in mice: importance of genetic background. *Kidney Int.* 2003;64(1):350-355.

53. Roopenian DC, Akilesh S. FcRn: the neonatal Fc receptor comes of age. *Nat Rev Immunol.* 2007; 7(9):715-725.

54. Kambham N, Markowitz GS, Appel GB, Kleiner MJ, Aucouturier P, D'agati VD. Heavy chain deposition disease: the disease spectrum. *Am J Kidney Dis.* 1999;33(5):954-962.

55. Bianchi G, Oliva L, Cascio P, et al. The proteasome load versus capacity balance determines apoptotic sensitivity of multiple myeloma cells to proteasome inhibition. *Blood.* 2009;113(13):3040-3049.

56. Cenci S, Oliva L, Cerruti F, et al. Pivotal Advance: Protein synthesis modulates responsiveness of differentiating and malignant plasma cells to proteasome inhibitors. *J Leukoc Biol.* 2012;92(5): 921-931.

57. Obeng EA, Carlson LM, Gutman DM, Harrington WJ Jr, Lee KP, Boise LH. Proteasome inhibitors induce a terminal unfolded protein response in multiple myeloma cells. *Blood.* 2006;107(12): 4907-4916.

58. Meister S, Schubert U, Neubert K, et al. Extensive immunoglobulin production sensitizes myeloma cells for proteasome inhibition. *Cancer Res.* 2007; 67(4):1783-1792.

59. Zhou P, Ma X, Iyer L, Chaulagain C, Comenzo RL. One siRNA pool targeting the λ constant region stops λ light-chain production and causes terminal endoplasmic reticulum stress. *Blood.* 2014;123(22):3440-3451.

60. Kastritis E, Terpos E, Dimopoulos MA. Current treatments for renal failure due to multiple myeloma. *Expert Opin Pharmacother.* 2013; 14(11):1477-1495.

61. Reece DE, Hegenbart U, Sanchorawala V, et al. Long-term follow-up from a phase 1/2 study of single-agent bortezomib in relapsed systemic AL amyloidosis. *Blood.* 2014;124(16):2498-2506.

62. Jaccard A, Comenzo RL, Hari P, et al. Efficacy of bortezomib, cyclophosphamide and dexamethasone in treatment-naïve patients with high-risk cardiac AL amyloidosis (Mayo Clinic stage III). *Haematologica.* 2014;99(9):1479-1485.